J Ther Eng, Vol. 12, No. 2, pp. 579−594, March, 2026

Journal of Thermal Engineering
Web page info: https://jten.yildiz.edu.tr
DOI: 10.14744/thermal.0001102

Research Article

Thermal and nanoscale relations of particles in mineral oil: An analysis of metallic and non-metallic particles

A.T. AKINSHILO[1,*], M.G. SOBAMOWO[1], L. KOLSI[2]

[1]Department of Mechanical Engineering, University of Lagos, Lagos, 100213, Nigeria
[2]Department of Mechanical Engineering, University of Ha'il, Ha'il, 55212, KSA

ARTICLE INFO

Article history
Received: 04 March 2025
Accepted: 15 July 2025

Keywords:
Heat Transfer; MHD; Micro Channel; Nanolayer; Particle Size

ABSTRACT

The mineral oil, a viscous liquid which is a derivative product from petroleum processing, having wide range of engineering applications, is studied in this paper. Thermal analysis of mineral oil in a microchannel incorporating nanoscale relations of metallic and non-metallic nanoparticles is investigated. The thermal effect on the nano layer is considered, which shows the relationship between the base fluid and nanoparticle. Also, the effect of nanoparticle size on the thermal layer is examined to understand the fluid performance under thermal load. The mechanics of the heat transfer and fluid transport are developed using coupled nonlinear system of higher partial differentials. They are analyzed using the Homotopy perturbation method upon transformation from partial to ordinary equations utilizing suitable similarity transforms. Results obtained from analysis show that optimum nanolayer thickness increases the surface layer of the nanoparticle, consequently increasing fluid temperature. Also, it is observed that the volume of the nanoparticle concentration from 1 to 8 % improves heat transfer and enhances shear stress at the wall boundary. The heat transfer rate using the graphite particles is higher compared to the copper particles, about 23 times more. Nanolayer thickness of 1nm and particle radius size within 5 to 20 nm studied shows good agreement with literature. Study may provide useful insight to tribologist and scientist interested in lubricant designs and process cooling.

Cite this article as: Akinshilo AT, Sobamowo MG, Kolsi L. Thermal and nanoscale relations of particles in mineral oil: an analysis of metallic and non-metallic particles. J Ther Eng 2026;12(2):579−594.

INTRODUCTION

The mineral oil, which is a viscous liquid obtained from the processing of petroleum products, is a colorless and odorless liquid. Mineral oil can be paraffinic, aromatic or naphthenic type. Having wide usage in refrigeration compressors, electric transformer cooling, amongst many other practical applications. Due to its thermal and viscous properties, researchers have studied this fluid in the bid to enhance its performance. Heat transfer cell was designed and developed by Eli [1] to accurately calculate the heat transport coefficient and thermal conductivity of the mineral oil

*Corresponding author.
*E-mail address: ta.akinshilo@gmail.com

This paper was recommended for publication in revised form by Editor-in Chief Ahmet Selim Dalkilic

at room temperature. The study reported shows that 40 nm copper oxide nanoparticles are not suitable with mineral oil as a base fluid for transformer cooling due to heat convection. The effect of chemically reactive species in steadily flowing mineral oil with aluminum oxide nanoparticles was analyzed numerically by Nazir et al. [2], where they observed that magnetic dipole and particle shape impact thermal conductivity. The concentration of nanoparticles on heat transfer and thermophysical properties of alumina nanosuspension for refrigeration application was studied by Jashi et al. [3]. They compared the experimentally observed results against model results for thermal conductivity and viscosity, which shows nanoparticle concentration has a direct effect on conductivity. Khoirudin et al. [4] analyzed mineral oil data to analyze the effect of breakdown voltage and thermal conductivity. Findings suggested that nanoparticles increase breakdown voltage and thermal conductivity. The impact of temperature reduction and loading capacity on distribution transformers using mineral oil was investigated by Taheri et al. [5], where they discovered addition of nanofluids increases loading capacity. Karaman et al. [6] presented their study on the influence of nanoparticles on temperature distribution in mineral oils. Study reveals that high thermal conductive fluids reduce thermal stress in oils. The rheological behavior of hybrid nanofluid (TiO_2 - Al_2O_3) in mineral oil was experimentally investigated by Shelton et al. [7]. It was reported that the ratio of nanoparticle mixture, concentration, and composition impacts the mineral oil rheological characteristics. Saman et al. [8] treated nanoparticles with plasmas to study their effects on breakdown strength, discharge resistance and thermo-physical properties of the mineral oil-based fluid. It is noted that the treatment of nanoparticles with plasma improved particle dispersion and stability, providing enhanced interaction between the base fluid and nanoparticles.

To conserve energy, reducing heat loss during fluid transfer becomes pertinent. The need to raise fluid thermal conductivity arises. This results in the inclusion of nanosized particles in pure fluid, which increases fluid thermal capacity as fluid is travelling through channels [9-10]. The nanofluid mixture finds relevant application in energy conservation, lubrication, fuel cells and micro-electronic processes [11-14]. Kiran et al. [15] used graphite in their study as an additive in lubricants, with results indicating inclusion of graphite led to a reduction of friction coefficient and deformation, preventing wear in steel. Also, copper nanoparticles were used by Guo et al. [16] in their study on tribological performance, with results showing copper reduces wear, friction coefficient and improves performance in engine oils. Dogonchi and Ganji studied the effect of nanofluid flow between stretchable and shrinkable plane walls, considering Brownian motion and thermal radiation [17-18]. It was presented that heat transfer rate is enhanced by stretching and radiation. Kumar et al. [19] studied the nanofluid flow over a bidirectional stretching surface, they showed that the boundary layer thickness of Cu-water is higher than methanol-Cu. The stability of nanoparticles and heat transfer of fluid over a moving and stationary thin needle was studied by Mabood and Akinshilo [20], where it was shown that increasing the volume concentration of nanoparticles decreases with fluid motion. Hdhiri et al. [21] studied nanofluid flow and convective heat transfer in the heated cavity, where it is shown that heat transfer is strongly dependent on Prandtls number.

Nanoscale relations between nanoparticles and base fluid have been receiving attention in recent times, owing to the inadequacy of established nanofluid models to justify the rise of the nanofluid thermal conductivity. Established conductivity models, including the Maxwell model [22] and the Hamilton and Crosser model [23], did not capture the effect of the nanolayer; consequently, could not justify the improvement in conductivity of nanofluid even at low volume concentration. The nanolayer effectively shows the connection between the base fluid and the nanoparticle as described by Acharya et al. [24]. The nanolayer shows the relationship between the base liquid and nanoparticle, showing a higher thermal conductivity than the nanoparticle and lower conductivity than the base fluid. The nanolayer and particle diameter were studied by Rana and Beg [25] using water-alumina nanofluid on inclined flow, where they concluded that nanoparticle diameter impacts thermal profile. The inter-particle spacing relations between particles were formulated by Graham [26] using a cell theory to derive the relation dependence of zero shear rate viscosity on volume concentration of uniformly dispersed solid spherical particles. Further, Gosunkanda et al [27] investigated the particle spacing effect in convective heat transfer through a cylindrical annulus.

The mineral oil has rigid but spherical particles that rotate during flow. Thermal fluidic mechanics comprises of macroscopic velocity field and a rotational motion component described in governing relations for micropolar fluids formulated by Eringen [28]. These governing relations are nonlinear, partial and higher-order systems of coupled equations. Simplified using similarity transforms into ordinary, higher-order differentials which can be analyzed using numerical or analytical techniques. Numerical methods such as Runge-Kutta, finite volume and finite elements methods have been used in the past. Analytical methods, including the Homotopy perturbation, Adomian decomposition, differential transformation, variation iteration, methods of weighted residuals, have been equally used to provide approximate analytical solutions to higher-order boundary value problems [29-31]. These methods suffer from their various limitations and rounding errors. However, the Homotopy perturbation method, an analytical method which provides ease of changing parameters, high procedural stability, yet has high convergence and accuracy, is used in this paper to study the thermal and fluid relation in the micro channel.

Nanoparticles' effect on fluids has been studied widely over the years, ranging from their use in heat transfer to fluid transport in various media, including channel flows, heat exchangers, solar collectors, and medical applications,

among others. The impact of improved thermal conduction leads to efficient heat transfer, energy conservation, improved thermal loading and less stress are significant and interesting observations. [32-39]. Studies presented in the literature do not capture both experimentally/ theoretically the relationship between the nanolayer and the particles for the mineral oil transport. It is not clear if this impact thermal distribution. Also, to what extent does this particle layer affect thermal conductivity, as it may explain the atypical rise in thermal conductivity.

In light of the above, this paper focus on theoretical study of the nanoscale relationship between the hydrodynamic nano layer, nanoparticle size, and inter-particle spacing of particles under thermal heating using metallic and non-metallic particles in mineral oil. To understand the anomalous increase in base fluid thermal conductivity upon nanoparticles inclusion and fluid performance under thermal load. Utilizing mineral oil (ISO grade 32), a mineral-based hydraulic fluid which serves as sealant, lubricant or coolant due to its inherent properties such as resistance to thermal breakdown, low temperature fluidity, amongst others. ISO grade 32 was selected over other grades including 46 and 68 due to its low viscosity of 30.4 cSt at 40 °C [40], which makes it a thin oil, flowing easily and suitable for static and high-powered rotating machinery. Copper and graphite as metallic and non-metallic nanoparticles respectively, aiding its stability and performance. The mechanics of the heat transfer and fluid transport are described with nonlinear, coupled models analyzed using the Homotopy perturbation method. Thereafter, the impact of rheological parameters are presented and discussed. Understanding derived from study may provide good insights into thermal transport designs of oil additives applications.

MODEL DEVELOPMENT

The mineral oil is characterized as a micropolar fluid, composed of arbitrary, rigid, and spherical oriented particles exhibiting micro rotations and flowing under steady-state conditions [41-42]. The magnetic field is applied perpendicularly to the microchannel, the flow maintains a constant speed through the channel. The nanofluid considered is a Newtonian fluid, with the temperature of the top and bottom wall taken as T_2 and T_1 respectively. As seen in Figure 1, the plate surface is perpendicular to the y-axis and normal to the x-axis. With the following dimension: length 50 mm, depth 40 mm, width 35 mm and depth between the plates 100 μm.

Considered Assumptions

The nanofluid mix is assumed to be incompressible and in non - thermal equilibrium (due to localized heating effect or thermal gradient in the channel). With respect to the above conditions, the continuity, momentum, micro-rotation and energy equations, which depict the concept of mass, momentum of flow, fluid particle rotation and energy conservation in and out of the channel, are reformulated as follows [43-44]:

Continuity equation

$$\frac{\partial u}{\partial x}+\frac{\partial v}{\partial y}=0, \tag{1}$$

Momentum equation

$$\rho_{nf}\left(u\frac{\partial u}{\partial x}+v\frac{\partial u}{\partial y}\right)=-\frac{\partial p}{\partial x}+(\mu_{nf}+\kappa)\left(\frac{\partial^2 u}{\partial x^2}+\frac{\partial^2 u}{\partial y^2}\right)+\kappa\frac{\partial N}{\partial y}-\sigma_f B_0^2 u, \tag{2}$$

$$\rho_{nf}\left(u\frac{\partial v}{\partial x}+v\frac{\partial v}{\partial y}\right)=-\frac{\partial p}{\partial x}+(\mu_{nf}+\kappa)\left(\frac{\partial^2 v}{\partial x^2}+\frac{\partial^2 v}{\partial y^2}\right)-\kappa\frac{\partial N}{\partial x}, \tag{3}$$

Micro-rotation equation

$$\rho_{nf} j\left(u\frac{\partial N}{\partial x}+v\frac{\partial N}{\partial y}\right)=-\kappa\left(2N+\frac{\partial u}{\partial y}-\frac{\partial v}{\partial x}\right)+\gamma_{nf}\left(\frac{\partial^2 N}{\partial x^2}+\frac{\partial^2 N}{\partial y^2}\right), \tag{4}$$

Energy equation

$$u\frac{\partial T}{\partial x}+v\frac{\partial T}{\partial y}=\frac{k_{nf}}{(\rho c_p)_{nf}}\left(\frac{\partial^2 T}{\partial x^2}+\frac{\partial^2 T}{\partial y^2}\right)-\frac{1}{(\rho c_p)_{nf}}\frac{\partial q_{rad}}{\partial y}+Q(T-T_\infty), \tag{5}$$

Where the magnetic field, pressure, velocity in the x and y directions, electric conductivity, temperature, viscosity vortex, micro-rotation velocity, radiative heat flux, spin gradient viscosity, and micro-inertia density respectively

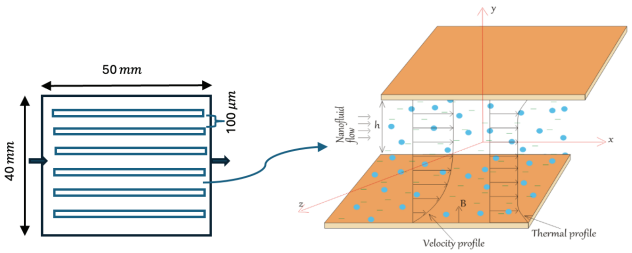

Figure 1a. Physical model and schematics of the problem.

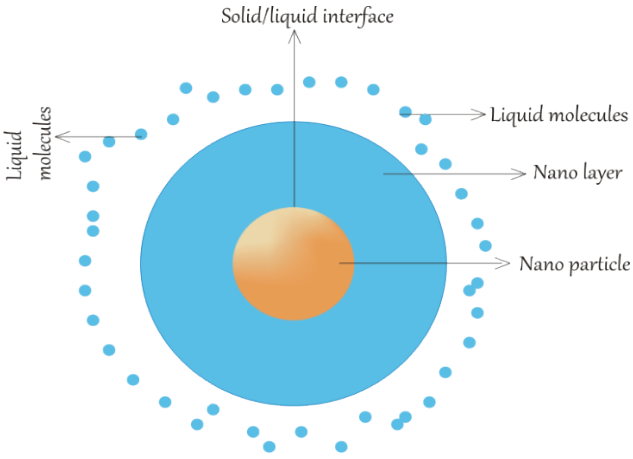

Figure 1b. Nanoparticle interfacial layer.

are represented as B_0, P, u, v, σ_f, T, κ, N, q_{rad}, j *and* γ_{nf}. Where $\gamma_{nf} = \left(\mu_{nf} + \frac{\kappa}{2}\right) j$.

Rooseland approximation is used to quantify the radiation heat transfer [45]. This approximation technique is confirmed to be valid for short radiation travel distances before scattering. Radiative heat transfer leaves the micropolar fluid before it is scattered within the thick optical fluid. The Rooseland approximation is formed to account for this effect. Radiative heat flux is presented as:

$$q_{rad.} = -\left(4\sigma^*/3k^*_{nf}\right)\frac{\partial T^4}{\partial y}. \quad (6)$$

The coefficient of absorption of the nanofluid is given as k^*_{nf} and the Stefan Boltzmann constant is represented as σ^*.More so, temperature of flow varies with distance. Therefore, the Taylor series is utilized in expanding temperature, T^4. T^4 is expanded about T_∞ by neglecting higher order terms.

$$T^4 \cong 4T_\infty^3 T - 3T_\infty^4. \quad (7)$$

Eq. (5) is rewritten:

$$u\frac{\partial T}{\partial x} + v\frac{\partial T}{\partial y} = \frac{k_{nf}}{(\rho c_p)_{nf}}\left(\frac{\partial^2 T}{\partial x^2} + \frac{\partial^2 T}{\partial y^2}\right) - \frac{16\sigma^* T_\infty^3}{3k^*_{nf}(\rho c_p)_{nf}}\frac{\partial^2 T}{\partial y^2} + Q(T - T_\infty), \quad (8)$$

The effective density and dynamic viscosity are given as ρ_{nf} and μ_{nf}, while $(\rho Cp)_{nf}$ and k_{nf} are the specific capacitance of heat and thermal conductivity of the nanofluid, respectively. The Eqs. (9) show the nanofluid parameters where the d is the diameter of the nanoparticle, Γ is the interfacial thickness layer, β is the nanolayer ratio, γ is the ratio of the interfacial layer thickness and particle size, ϕ is the nanoparticle volume and electrical conductivity σ_{nf}; these are introduced as [24]. The liquid-solid interfacial layer and nanoparticle diameter play a crucial role in the amplified thermal conductivity. The classical thermal conductivity relations proposed by Maxwell [22] and Hamilton and Crosser [23] were not utilized in this paper since the relations do not consider the interfacial layer and nanoparticle diameter in their thermal conductivity relations. Consequently, their model did not sufficiently capture the anomalous increased nanofluid thermal conductivity. Also, the relationship between the nanofluid viscosity and the pure fluid viscosity is examined using the dynamic viscosity model formulated by Graham [26] and Gasukonda et al. [27], where ψ the inter-particle spacing between the particles is considered. This gives better insight into the rheological properties of the nanoparticles and the base fluid. The thermophysical properties of the fluid and nanoparticles are expressed in Table 1.

$$\begin{aligned}
&\rho_{nf} = (1-\phi)\rho_f + \phi\rho_s,\\
&\left(\rho C_p\right)_{nf} = (1-\phi)\left(\rho C_p\right)_f + \phi\left(\rho C_p\right)_s,\\
&\frac{\mu_{nf}}{\mu_f} = \left(1 + 2.5\phi + 4.5\left(\frac{1}{2\psi/d(2+2\psi/d)(1+2\psi/d)^2}\right)\right),\\
&\frac{k_{nf}}{k_f} = \frac{(k_s-\beta k_f)\phi\beta(2\gamma_1^3-\gamma_2^3+1)+(k_s-2\beta k_f)\gamma_1^3[\phi\gamma_2^3(\beta-1)+1]}{\gamma_1^3(2\gamma_1^3-\gamma_2^3+k_s)+(\beta k_f-k_s)\phi(\gamma_1^3+\gamma_2^3-1)}.\\
&\text{Where } \gamma_1 = 1+\frac{\Gamma}{2d},\ \gamma_2 = 1+\frac{\Gamma}{d}
\end{aligned} \quad (9)$$

Given the microelements rotational factor close to the wall as s. Hence, s = 0, denotes there is no microelements close to the wall and particle flow concentration as occurred. Turbulent and weak concentration occurs at s = 1 and s = 0.5, respectively. Fluid suction and injection occur at $v_0 > 0$ and $v_0 < 0$.

The principle of energy conservation is satisfied at the nanoscale with the no-slip and no thermal jump condition, due to velocity and temperature of the fluid layer in contact with the channel are similar i.e. no discontinuity in the channel. This is presented in Eq. (10) below:

$$\begin{aligned}
&u = 0,\ v = -v_0 \quad N = -s\left.\frac{\partial u}{\partial y}\right|_{y=-h} \quad T = T_1,\ At\ \ y = -h,\\
&u = 0,\ v = v_0, \quad N = -s\left.\frac{\partial u}{\partial y}\right|_{y=+h} \quad T = T_2,\ At\ \ y = +h.
\end{aligned} \quad (10)$$

With similarity variables given as:

$$\begin{aligned}
&\eta = \frac{y}{h}, u = -\frac{v_0 x}{h}f'(\eta), N = \frac{v_0 x}{h^2}g(\eta), v = v_0 f(\eta),\\
&\theta = (T-T_1)/(T_2-T_1), T_2 = T_1 + Ax.
\end{aligned} \quad (11)$$

The similarity variables in Eq. (11) is substituted into the governing relations Eq. (1-4,8) and boundary conditions Eq. (10). Neglecting the pressure gradient in the governing relations, the equations are transformed into an ordinary differentials. To further simplify the problem, it is non-dimensionalized into physical parameters and simply expressed as Eq.(12-15) below, with the physical parameters given as Eq. (16):

Table 1. Thermal physical properties of nanofluid. [13, 46, 47]

	$\rho(Kg/m^3)$	Cp (J/KgK)	$k(W/mK)$
Copper (Cu)	8933	385	401
Graphite	2210	709	1950
Mineral oil (ISO grade 32)	861.55	1867.31	0.1345

$$\left(1+\left(1+2.5\phi+4.5\left(\frac{1}{2\psi/d(2+2\psi)(1+2\psi/d)^2}\right)\right)\chi\right)f^{iv} - \left(1+2.5\phi+4.5\left(\frac{1}{2\psi/d(2+2\psi)(1+2\psi/d)^2}\right)\right)\chi g'' - \left(1-\phi+\frac{\rho_s}{\rho_f}\phi\right)\left(1+2.5\phi + 4.5\left(\frac{1}{2\psi/d(2+2\psi)(1+2\psi/d)^2}\right)\right)Re(ff''' - f'f'') - \left(1+2.5\phi+4.5\left(\frac{1}{2\psi/d(2+2\psi)(1+2\psi/d)^2}\right)\right)Mf'' = 0, \quad (12)$$

$$\left(1+\left(\frac{1+2.5\phi+4.5}{2}\left(\frac{1}{2\psi/d(2+2\psi)(1+2\psi/d)^2}\right)\right)\chi\right)g'' + \left(1+2.5\phi+4.5\left(\frac{1}{2\psi/d(2+2\psi)(1+2\psi/d)^2}\right)\right)\chi(f''-2g) - \left(1-\phi+\frac{\rho_s}{\rho_f}\phi\right)\left(1+2.5\phi + 4.5\left(\frac{1}{2\psi/d(2+2\psi)(1+2\psi/d)^2}\right)\right)Re(fg'-gf') = 0, \quad (13)$$

$$\theta''+\left((1-\phi)+\frac{(\rho c_p)_s}{(\rho c_p)_f}\phi\right)\left(\frac{3}{3+4Nr}\right)\frac{k_f}{k_{nf}}PrRe(f'\theta-f\theta')+\xi\theta=0. \quad (14)$$

The boundary conditions are presented as:

$$f(-1)=-1,\ f'(-1)=0,\ f(+1)=1,\ f'(+1)=0,\quad g(-1)=0,\ g(+1)=0,\quad \theta(-1)=0,\ \theta(+1)=1. \quad (15)$$

Where Reynold number is defined as Re, magnetic parameter is denoted as M. Prandtl number is shown as Pr, radiation parameter is Nr and heat generation is given as ξ, micropolar parameter as χ accounts for the particle micro-rotation throughout the fluid. Justifying the colloidal stability of fluid elements to remain dispersed. The non-dimensional parameters are presented as follows:

$$\chi=\kappa/\mu_f,\ P_r=\mu_f C_{p,f}/k_f,\ \mathrm{Nr}=k_{nf}k^*_{nf}/4\sigma^*T_\infty^3,\quad Re=\rho_f v_0 h/\mu_f,\ M=\sigma_f B_0^2 h^2/\mu_f,\ \xi=\frac{Q(\rho C_P)_{nf}}{(T-T_\infty)}. \quad (16)$$

Fluid undergoes suction when Re > *0*; similarly, injection flow is seen when Re < *0*. Important engineering parameters of physical impact are the skin friction and Nusselt number, which are presented as:

$$C_f^*=-\left(\frac{2}{\rho_f u^2}\right)(\mu_{nf}+\kappa)\left.\frac{\partial u}{\partial y}\right|_{y=-h},\quad Nu^*=-\left(\frac{h}{k_f(T_2-T_1)}\right)\left(k_{nf}+\frac{16\sigma^*T_\infty^3}{3k^*_{nf}}\right)\left.\frac{\partial T}{\partial y}\right|_{y=-h}. \quad (17)$$

With the aid of similarity variables in Eq. (11), we can write Eq (17) as:

$$C_f=\left|\left(\frac{\mu_{nf}}{\mu_f}+\chi\right)f''(-1)\right|,\quad Nu=\left|\frac{k_{nf}}{k_f}\left(\frac{3+4Nr}{3}\right)\theta'(-1)\right|. \quad (18)$$

The concentration ratio of pure fluid to solid particles is considered low. Therefore, the nanoparticle concentration volume range of 1-8% of the total volume is selected, which is within reasonable range of nanoparticle concentration for microfluidics [48]. The flow condition is for steady/laminar flow. Therefore, Reynolds number were selected over a reasonable range $5 \le Re \le 20$ for entry region length with no surface roughness [49], the micro polar parameter is selected over a low range $1 \le \chi \le 8$ for low micro-rotation of fluid particles. The nanolayer range is selected over a range $0.45 \le h \le 1$ for spherical-shaped particles. This is based on molecular dynamics simulation verified with experiment by Yu et al [50] and consistent with analysis reported by Yu and Choi [51]. The diameter range varies between 10 nm ≤ d ≤ 40nm for the nanoparticles. The nanoparticles induce depletion in the nanolayer region if it is ten times larger than the molecular diameter of water. This is valid for mineral oil (ISO grade 32) having a density lower than water [39,52-54]. Other parameters used are selected over a reasonable range from the values expressed in [24].

Analytical Solution

The fluid transport and heat transfer through the channel, considering the interfacial hydrodynamic layer, diameter of the nano-sized particle and thermal radiation, is studied using the Homotopy perturbation method (HPM). The fundamentals and principles of HPM, an analytical method, have been extensively described in [55-56] by J.H. He. HPM, a method of approximate analytical solution with fast convergence and procedural stability is the method selected to obtain the solutions to the system of coupled nonlinear boundary value problem. Applying the HPM procedure as discussed above to the governing equations, the Homotopy of the Eqs. (12-14) can be constructed as follows

$$(p,\eta)=(1-p)\left[\frac{d^4f}{\partial\eta^4}\right] + p\left[\begin{array}{l}\frac{d^4f}{d\eta^4}-\left(1+2.5\phi+4.5\left(\frac{1}{\frac{2\psi}{d(2+2\psi)\left(1+\frac{2\psi}{d}\right)^2}}\right)\right)\chi\frac{d^2g}{d\eta^2}\\ -\left(1-\phi+\frac{\rho s}{\rho f}\phi\right)\left(1+2.5\phi+4.5\left(\frac{1}{\frac{2\psi}{d(2+2\psi)\left(1+\frac{2\psi}{d}\right)^2}}\right)\right)\\ Re\left(f\frac{d^3f}{d\eta^3}-f\frac{d^2f}{d\eta^2}\right)-\\ \left(1+2.5\phi+4.5\left(\frac{1}{\frac{2\psi}{d(2+2\psi)\left(1+\frac{2\psi}{d}\right)^2}}\right)\right)M^2\frac{d^2f}{d\eta^2}\end{array}\right] / \left(1+\left(1+2.5\phi+4.5\left(\frac{1}{2\psi/d(2+2\psi)(1+2\psi/d)^2}\right)\right)\chi\right)=0 \quad (19)$$

$$H_2(p,\eta) = (1-p)\left[\frac{d^2g}{d\eta^2}\right] + p\left[\frac{d^2g}{d\eta^2} - \left(1+2.5\phi+4.5\left(\frac{\frac{1}{2\psi}}{d(2+2\psi)\left(1+\frac{2\psi}{d}\right)^2}\right)\right)\chi\left(\frac{d^2f}{d\eta^2}-2g\right) - \left(1-\phi+\frac{\rho s}{\rho f}\phi\right)(1-\phi)^{2.5}\,Re\left(f\frac{dg}{d\eta}-g\frac{df}{d\eta}\right)\right] \Big/ \left(1+\left(\frac{1+2.5\phi+4.5}{2}\left(\frac{1}{2\psi/d(2+2\psi)(1+2\psi/d)^2}\right)\right)\chi\right) = 0, \quad (20)$$

$$H_3(p,\eta) = (1-p)\left[\frac{d^2\theta}{d\eta^2}\right] + p\left[\frac{d^2\theta}{d\eta^2} + \left((1-\phi)+\frac{(\rho C_p)_s}{(\rho C_p)_f}\phi\right)\left(\frac{3N}{3N+4}\right)\frac{k_f}{k_{nf}}PrRe\left(\frac{df}{d\eta}\theta - f\frac{d\theta}{d\eta}\right)+\xi\theta\right] = 0. \quad (21)$$

Substituting the homotopy of the governing Eq. (19-21) in the power series (P) for velocity, rotation and temperature presented in Eq. (22) below:

$$f = P^0 f_0 + P^1 f_1 + P^2 f_2 + \ldots \quad (22a)$$

$$g = P^0 g_0 + P^1 g_1 + P^2 g_2 + \ldots \quad (22b)$$

$$\theta = P^0\theta_0 + P^1\theta_1 + P^2\theta_2 + \ldots \quad (22c)$$

These are expanded from the zeroth to the second order for accuracy and convergence of the analytical solutions. Eq. (22a) is substituted into (19) for the velocity profile and selected at the various order (zeroth to second) yields

$$p^0: \frac{d^4f_0}{d\eta^4} \quad (23a)$$

$$p^1: \frac{\left[\frac{d^4f_1}{d\eta^4} - \left(1+2.5\phi+4.5\left(\frac{\frac{1}{2\psi}}{d(2+2\psi)\left(1+\frac{2\psi}{d}\right)^2}\right)\right)\chi\frac{d^2g_0}{d\eta^2} - \left(1-\phi+\frac{\rho s}{\rho f}\phi\right)\left(1+2.5\phi+4.5\left(\frac{\frac{1}{2\psi}}{d(2+2\psi)\left(1+\frac{2\psi}{d}\right)^2}\right)\right)Re\left(f_0\frac{d^3f_0}{d\eta^3} - f_0\frac{d^2f_0}{d\eta^2}\right) - \left(1+2.5\phi+4.5\left(\frac{\frac{1}{2\psi}}{d(2+2\psi)\left(1+\frac{2\psi}{d}\right)^2}\right)\right)M^2\frac{d^2f_0}{d\eta^2}\right]}{\left(1+\left(1+2.5\phi+4.5\left(\frac{1}{2\psi/d(2+2\psi)(1+2\psi/d)^2}\right)\right)\chi\right)} \quad (23b)$$

$$p^2: \frac{\left[\frac{d^4f_2}{d\eta^4} - \left(1+2.5\phi+4.5\left(\frac{1}{2\psi/d(2+2\psi)(1+2\psi/d)^2}\right)\right)\chi\frac{d^2g_1}{d\eta^2} - \left(1-\phi+\frac{\rho s}{\rho f}\phi\right)\left(1+2.5\phi+4.5\left(\frac{1}{2\psi/d(2+2\psi)(1+2\psi/d)^2}\right)\right)Re\,f_0\frac{d^3f_1}{d\eta^3} + \left(1-\phi+\frac{\rho s}{\rho f}\phi\right)(1-\phi)^{2.5}\,Re\,f_0\frac{d^2f_1}{d\eta^2} - \left(1+2.5\phi+4.5\left(\frac{1}{2\psi/d(2+2\psi)(1+2\psi/d)^2}\right)\right)M\frac{d^2f_1}{d\eta^2}\right]}{\left(1+\left(1+2.5\phi+4.5\left(\frac{1}{2\psi/d(2+2\psi)(1+2\psi/d)^2}\right)\right)\chi\right)} \quad (23c)$$

Eq. (22b) is substituted into (20) for the rotation profile and selected at the various order (zeroth to second) yields

$$p^0: \frac{d^2g_0}{d\eta^2} \quad (24a)$$

$$p^1: \frac{\left[\frac{d^2g_1}{d\eta^2} - \left(1+2.5\phi+4.5\left(\frac{1}{2\psi/d(2+2\psi)(1+2\psi/d)^2}\right)\right)\chi\left(\frac{d^2f_0}{d\eta^2}-2g_0\right) - \left(1-\phi+\frac{\rho s}{\rho f}\phi\right)\left(1+2.5\phi+4.5\left(\frac{1}{2\psi/d(2+2\psi)(1+2\psi/d)^2}\right)\right)Re\left(f_0\frac{dg_0}{d\eta} - g_0\frac{df_0}{d\eta}\right)\right]}{\left(1+\frac{\left(1+2.5\phi+4.5\left(\frac{1}{2\psi/d(2+2\psi)(1+2\psi/d)^2}\right)\right)}{2}\chi\right)} \quad (24b)$$

$$p^2: \frac{\left[\frac{d^2g_2}{d\eta^2} + \left(1+2.5\phi+4.5\left(\frac{1}{2\psi/d(2+2\psi)(1+2\psi/d)^2}\right)\right)\chi\frac{d^2f_1}{d\eta^2} - 2g_1 - \left(1-\phi+\frac{\rho s}{\rho f}\phi\right)\left(1+2.5\phi+4.5\left(\frac{1}{2\psi/d(2+2\psi)(1+2\psi/d)^2}\right)\right)Re\,f_0\frac{dg_1}{d\eta} + \left(1-\phi+\frac{\rho s}{\rho f}\phi\right)\left(1+2.5\phi+4.5\left(\frac{1}{2\psi/d(2+2\psi)(1+2\psi/d)^2}\right)\right)Reg_0\frac{df_1}{d\eta}\right]}{\left(1+\frac{\left(1+2.5\phi+4.5\left(\frac{1}{2\psi/d(2+2\psi)(1+2\psi/d)^2}\right)\right)}{2}K\right)} \quad (24c)$$

Eq. (22c) is substituted into (21) for the temperature profile and selected at the various order (zeroth to second) yields

$$p^0: \frac{d^2\theta_0}{d\eta^2} \quad (25a)$$

$$p^1: \frac{d^2\theta_1}{d\eta^2} + \left((1-\phi)+\frac{(\rho C_p)_s}{(\rho C_p)_f}\phi\right)\left(\frac{3Nr}{3Nr+4}\right)\frac{k_f}{k_{nf}}PrRe\left(\frac{df_0}{d\eta}\theta_0 - f_0\frac{d\theta_0}{d\eta}\right)+\xi\theta_0 \quad (25b)$$

$$p^2: \frac{d^2\theta_2}{d\eta^2} + \left((1-\phi)+\frac{(\rho C_p)_s}{(\rho C_p)_f}\phi\right)\left(\frac{3Nr}{3Nr+4}\right)\frac{k_f}{k_{nf}}PrRe\left(\frac{df_0}{d\eta}\theta_1 - f_0\frac{d\theta_1}{d\eta}\right)+\xi\theta_1 \quad (25c)$$

The Eq. (23-25) is analyzed using the boundary condition Eq. (15) at the various orders of the homotopic series. The final solution for the velocity, rotation and temperature profile at the various order (zero to second) are summed up and reported as follow in Eq. (26)-(28).

$$\begin{aligned} f = {} & \frac{3\eta}{2} - \frac{\eta^3}{2} + \Big(-(Re/140 - Re\,\phi/140) \\ & /8\chi\left(1+2.5\phi+4.5\left(\frac{1}{2\psi/d(2+2\psi/d)(1+2\psi/d)^2}\right)\right)+8\Big) - \\ & (Re\,\phi\,\rho s)/\left(1120\rho f\left(\chi\left(1+2.5\phi+4.5\left(\frac{1}{2\psi/d(2+2\psi/d)(1+2\psi/d)^2}\right)\right)+7\right)\right. \\ & +(Re\,\phi\,\rho s)/\left(560\rho f\left(\chi\left(1+2.5\phi+4.5\left(\frac{1}{2\psi/d(2+2\psi/d)(1+2\psi/d)^2}\right)\right)+1\right)\right)\eta^7 \\ & +\left(\frac{((3\,Re)/40 -}{(3\,Re\,\phi)/40}\right) \\ & /\left(6\chi\left(1+2.5\phi+4.5\left(\frac{1}{2\psi/d(2+2\psi/d)(1+2\psi/d)^2}\right)\right)+6\right) \\ & +(Re\,\phi\,\rho s)/\left(80\rho f(\chi\left(1+2.5\phi+4.5\left(\frac{1}{2\psi/d(2+2\psi/d)(1+2\psi/d)^2}\right)\right)+1)\right)\eta^6 \\ & +(-((3\,Re)/16 - (3\,Re\,\phi) \\ & /16 + \left(M\left(1+2.5\phi+4.5\left(\frac{1}{2\psi/d(2+2\psi/d)(1+2\psi/d)^2}\right)\right)\right. \\ & /8)\left(5\chi\left(\begin{matrix}1+2.5\phi \\ +4.5\left(\frac{1}{2\psi/d(2+2\psi/d)}\right) \\ (1+2\psi/d)^2\end{matrix}\right)\right)+5\Big) \\ & +\ldots. \end{aligned} \quad (26)$$

$$
\begin{aligned}
g = {} & \frac{\eta}{2} + \frac{1}{2}\eta^4\Bigg[\Bigg(\Bigg(Re\left(1 + 2.5\phi + 4.5\left(\frac{1}{2\psi/d(2+2\psi/d)(1+2\psi/d)^2}\right)\right) \\
& /2\left(Re\,\phi\left(4.5\left(\frac{1}{2\psi/d(2+2\psi/d)}\right)\right)\right)\Bigg)/2\Bigg) \\
& /\left(4(\chi\left(1 + 2.5\phi + 4.5\left(\frac{1}{2\psi/d(2+2\psi/d)(1+2\psi/d)^2}\right)\right) + 2)\right) \\
& + \left(Re\,\phi\,ps\left(4.5\left(\frac{1}{2\psi/d}\right)\right)\right)\Bigg] \\
& /\left(8\rho f\left(\chi\left(1 + 2.5\phi + 4.5\left(\frac{1}{2\psi/d(2+2\psi/d)(1+2\psi/d)^2}\right)\right) + 2\right)\right) + \\
& \eta^5\Bigg(\Bigg(\Bigg(\Bigg(Re\left(\frac{1}{2\psi/d(2+2\psi/d)(1+2\psi/d)^2}\right)\Bigg)/4 - \left(Re\,\phi\left(1 + 2.5\phi + 4.5\left(\frac{1}{2\psi/d(2+2\psi/d)(1+2\psi/d}\right.\right.\right.\right. \\
& /4 \\
& /\left(5\left(\chi\left(1 + 2.5\phi + 4.5\left(\frac{1}{2\psi/d(2+2\psi/d)(1+2\psi/d)^2}\right)\right) + 2\right)\right) \\
& + \left(Re\,\phi\,ps\left(1 + 2.5\phi + 4.5\left(\frac{1}{2\psi/d(2+2\psi/d)}\right)\right)\right)\Bigg) \\
& /\left(20\rho f\left(\chi\left(1 + 2.5\phi + 4.5\left(\frac{1}{2\psi/d(2+2\psi/d)(1+2\psi/d)^2}\right)\right) + 2\right)\right) \\
& + \eta^2((2\chi\left(1 + 2.5\phi + 4.5\left(\frac{1}{2\psi/d(2+2\psi/d)}\right)\right) \\
& -\left(3\,Re\left(1 + 2.5\phi + 4.5\left(\frac{1}{2\psi/d(2+2\psi/d)(1+2\psi/d)^2}\right)\right)\right))/2 \\
& + \left(3\,Re\,\phi\,ps\left(1 + 2.5\phi + 4.5\left(\frac{1}{2\psi/d(2+2\psi/d)}\right)\right)\right)\Bigg)/ \\
& (4\rho f(\chi\left(1 + 2.5\phi + 4.5\left(\frac{1}{2\psi/d(2+2\psi/d)(1+2\psi/d)^2}\right)\right) + 2))) \\
& - (\left(Re\left(1 + 2.5\phi + 4.5\left(\frac{1}{2\psi/d(2+2\psi/d)}\right)\right)\right)/2 \\
& +\ldots.
\end{aligned} \tag{27}
$$

$$
\begin{aligned}
\theta = {} & \begin{pmatrix}
(\eta+1)320k_{nf}\rho\,C_f + 240Nrk_{nf}\rho\,C_f + 71Nr\,PrRe\,\xi\,k_f\rho\,C_f(1-\phi) \\
+ 71Nr\,PrRe\,\xi\,k_f\rho\,C_s\,\phi - 34Nr\,PrR \\
4N\,PrRe\,\xi\,\eta^3k_f\rho\,C_f + 11Nr\,PrRe\,\xi\,\eta^4k_f\rho\,C_f \\
+ 4N\square\square\,PrRe\,\xi\,\eta^5k_f\rho\,C_f - 56Nr\,PrRe\,\xi\,\eta k_f\rho\,C_f(1-\phi) \\
- 56Nr\,PrRe\,\xi\,\eta k_f\rho\,C_s(1-\phi) + 34Nr\,PrRe\,\xi\,\eta^2k_f\rho\,C_f\,\phi \\
- 4Nr\,PrRe\,\xi\,k_f\rho\,C_f\,\eta^3\,\phi - 11Nr\,PrRe\,\xi\,\eta^4k_f \\
-4Nr\,PrRe\,\xi\,\eta^5k_f\rho\,C_f\,\phi - 34Nr\,PrRe\,\xi\,\eta^2k_f\rho\,C_s\,\phi \\
+ 4Nr\,Pr\,\xi\,\eta^3k_f\rho\,C_s\,\phi + 11Nr\,PrRe\,\xi\,\eta^4k_f\rho\,C_s\,\phi \\
+4Nr\,PrRe\,\xi\,\eta^5k_f\rho\,C_f\,\phi
\end{pmatrix} \\
& /\left(160k_{nf}\rho\,C_f(3N+4)\right) + \frac{\eta}{2} + 0.5 + \ldots..
\end{aligned} \tag{28}
$$

As the second-order coefficient for velocity, rotation and temperature in Eqs. (26 - 28) are too voluminous to be written. They are expressed in tables and graphically in the results. The analytical solution obtained from this study was further solved numerically using the Runge-Kutta Fehlberg method to validate the obtained analytical solution through HPM. As observed from Table 2, close-range solutions are observed. This proves the accuracy of the current study with the flow process of the analysis as described in Figure 2.

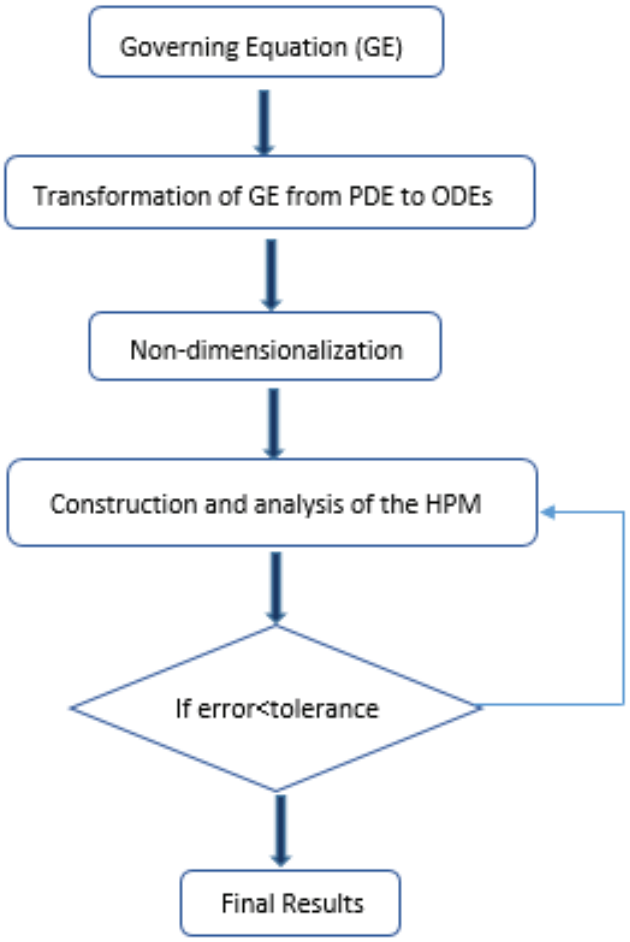

Figure 2. Flow chart of the analysis.

RESULTS AND DISCUSSION

Based on the analytical solutions reported in the previous section, with reference to underlying assumptions and

Table 2. Comparison of values for temperature profile with numerical method

η	$\theta(\eta)$ RKF-45	$\theta(\eta)$ Present study	Error	RMSD
0	0.0000	0.000000000	0.00000000	0
0.2	0.2000	0.200001085	0.00001085	5.42×10^{-7}
0.4	0.4000	0.400001653	0.00001653	8.26×10^{-7}
0.6	0.6000	0.600001598	0.00001598	7.98×10^{-7}
0.8	0.8000	0.800009426	0.00009426	4.71×10^{-6}
1.0	1.0000	1.000000000	0.00000000	0

Table 3. Impact of the Nusselt number on varying parameters of χ=M=1, Re=5, Nr=10 and Pr=10.

Γ	ϕ	ξ	d	ψ	Nusselt1 10^6	Nusselt2 10^6
0.5	0	2	10	1	**1.3162**	**31.0648**
0.75	0.02				**1.3212**	**31.1911**
1	0.04				**1.3262**	**31.3174**
	0.06				**1.3313**	**31.4436**
		4	30	1	**1.3320**	**31.4444**
		6	40	1.5	**1.3328**	**31.4452**

accuracy of the method utilized. These are used to generate and discuss plots here. These show graphically the heat transfer and flow through the microchannel. Reported plots are obtained at a constant value Re = 5, M = 1, Γ = 1, d = 10, β = 1.2, χ = ξ = 1, Nr = 10, Pr = 10, ϕ = 0.01, ψ = 1.5 unless stated otherwise. The validity of the analytical solution obtained in this work, is compared with the Runge Kutta Fehlberg (RKF-45) numerical solution for the simple case. As observed in Table 2, good agreements are established between the methods of solution. Also, the root mean square deviation (RMSD), as a method of quantifying uniformity, shows the temperature distribution pattern is uniform/similar having low values. The impact of the nanolayer between the nanoparticle and fluid, as well as particle size, heat generation, particle volume, and inter-particle spacing, is shown in Table 3. Nusselt[1] refers to heat transfer using copper nanoparticles, and Nusselt[2] using graphite particles. As seen, the rheological parameters have large effects on heat transfer. The effect of large nanoparticle volume and nanolayer on heat transfer, setting constant other rheological parameters, shows increasing heat transfer, which can be physically explained due to higher particle concentration enhancing fluid thermal conductivity and contact area, consequently, heat exchange increases. With larger inter-particle spacing, which decreases particle agglomeration, this impacts thermal conductivity, decreasing fluid heat transfer. Also, a large particle size decreases fluid transfer as it absorbs more heat. The heat transfer rate using graphite particles is very high compared to copper particles, this agrees with the results given by Gosunkanda et al. [27]. However, increasing thermal heat generation ($4 \leq \xi \leq 6$) minimizes the rate of heat transfer. From analysis heat transfer rate of the graphite is about 23 times more compared to copper. This rate is obtained on the basis of constant thermal conductivity of copper i.e. oxidation does not occur. Actually, exposure of copper particles to mineral oil will form a thin oxide layer on the particle surface. This will further reduce conductive properties of copper to < 8.3 % [57]. Increasing the rate derived. Similarly, graphite as it flows through the channel, due to the effect of weak bonds by Van der Waals forces shows inter layer sliding. This impacts the thermal conductivity, hindering heat flow [58]. Consequently, reducing heat transfer rate. Therefore, the derived rate expressed will decrease. The impact of the magnetic field is shown in Figure 3, as seen fluid velocity distribution rises from the bottom plate. The fluid approaches the center of the plate $\eta = 0$, a reverse trend is observed showing velocity drop. This is due to the interaction between the Lorentz force field (which increases due to magnetic intensity) with the micro polarity of the fluid. The rising field intensity along the region of flow resists the flow with rotating particles, reducing fluid streamline patterns. This force is perpendicular to the flow direction and acts as a barrier, altering the flow pattern. The volume concentration effect on fluid transport is shown in Figure 4. This shows an increasing volume concentration of nanoparticles from 1 – 8 %, velocity distribution decreases, which is because of abating thickness in the momentum boundary layer during flow transport. It is observed in Figure 5 that flow declines with rising micro-rotation of fluid particles during flow, as colliding rotating particles lower the kinematic viscosity.

The effect of the magnetic parameter on the fluid micro rotation is reported in Figure 6. This shows rotation of micro particles reduces at the lower plate. Towards the mid – plate rotation of fluid particles rises to the upper plate. This is because of the applied magnetic field known as the Lorentz force through the porous wall, which resists fluid

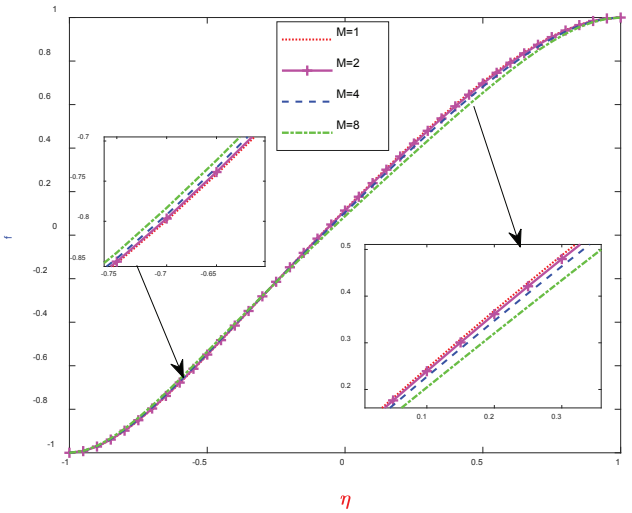

Figure 3. Effect of magnetic parameter on velocity profile.

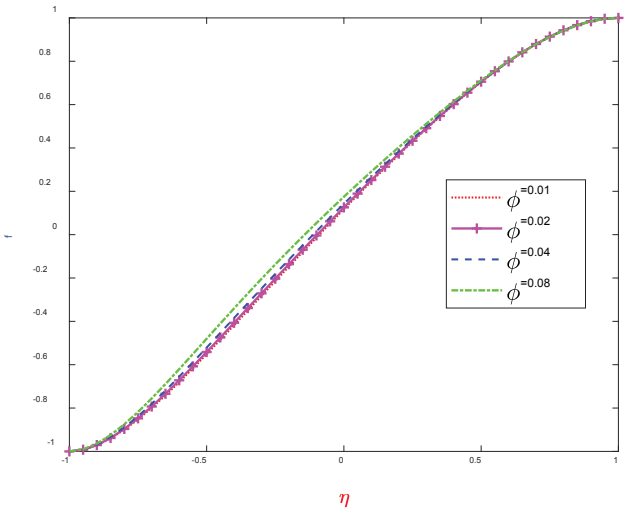

Figure 4. Effect of volume concentration on velocity profile.

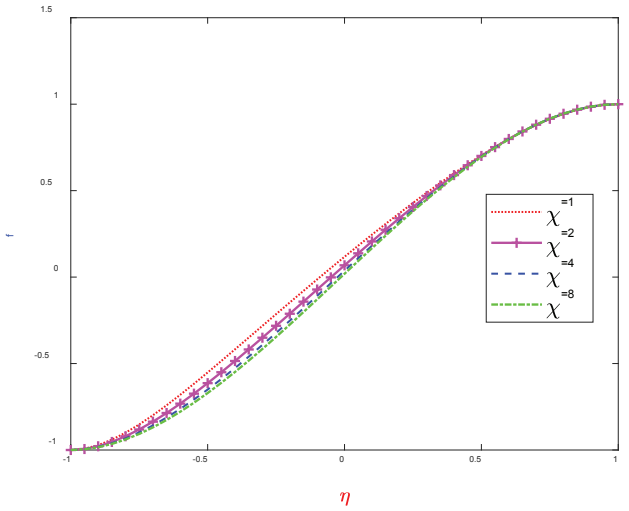

Figure 5. Effect of micropolar parameter on velocity profile.

flow towards the boundary. Enhancement of the nanoparticle volume reduces rotation of fluid particles as seen in Figure 7. This causes high energy exchange between molecules, decreasing the thickness of the boundary layer, consequently reducing micro rotation of fluid particles, towards the upper plate around $0.4 \geq \eta \geq 0.8$ a slight rise in particle rotation is noticed. The effect of increasing micropolar parameter on rotation is shown in Figure 8. As seen in the graphical plot, there is a sharp rise in fluid rotation due to a rise in vortex viscosity. The rotation rises significantly towards the bottom plate, then declines towards the upper plate. The Reynolds parameter impact on the rotation profile is seen in Figure 9, which shows a rise in rotation of fluid particles till about $-1 \geq \eta \geq -0.4$, and thereafter a sharp decline in rotation is noticed up to the wall of the upper plate, which is due to the dominance of inertia fluid forces in this region.

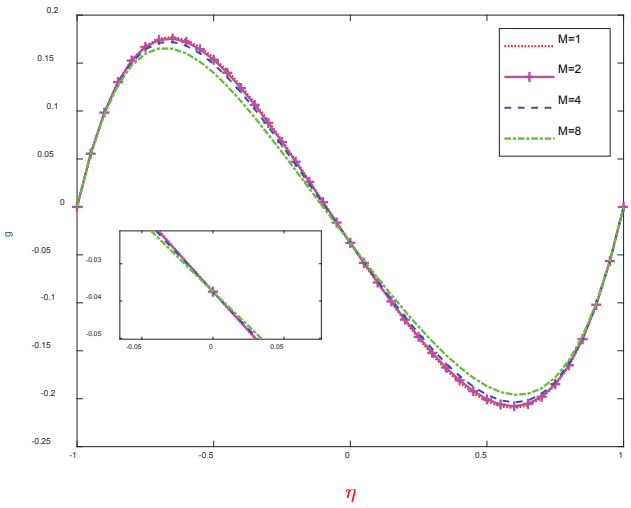

Figure 6. Effect of magnetic parameter on rotation profile.

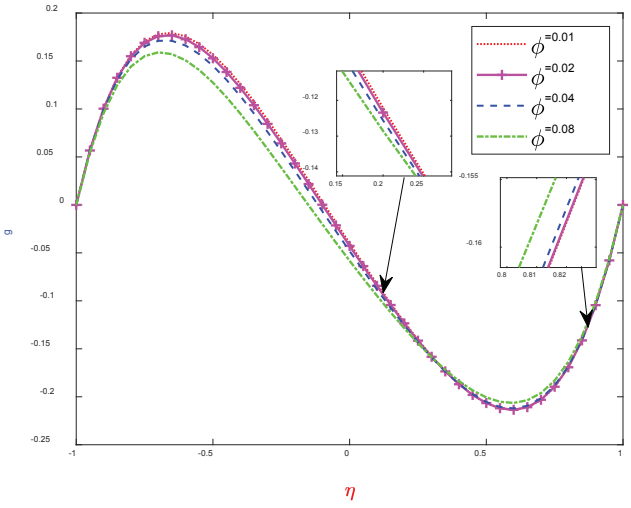

Figure 7. Effect of volume concentration on rotation profile.

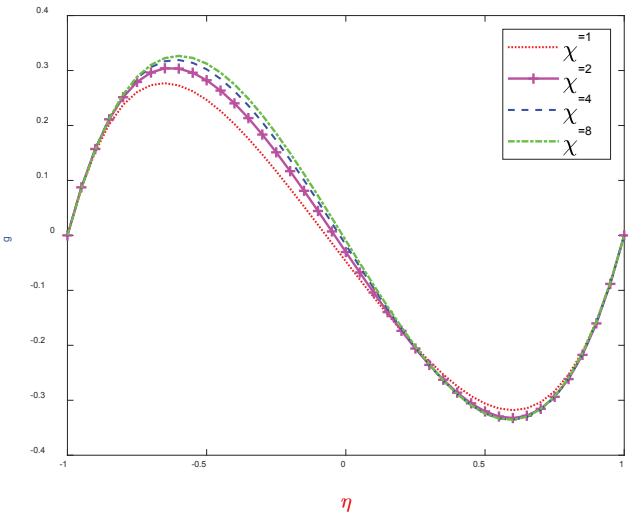

Figure 8. Effect of micropolar parameter on rotation profile.

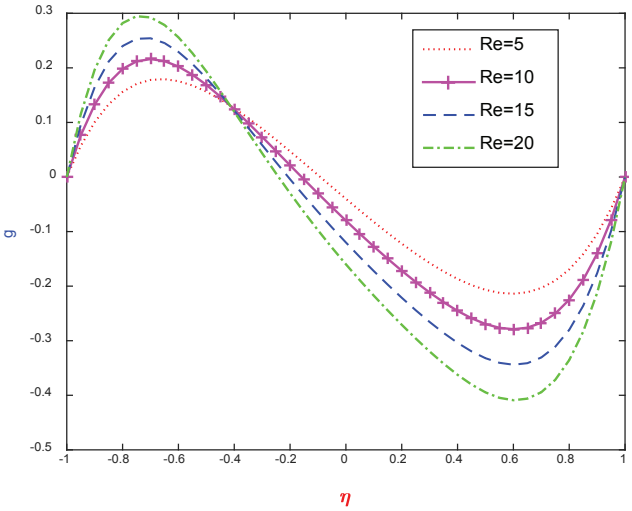

Figure 9. Effect of Reynolds number on rotation profile.

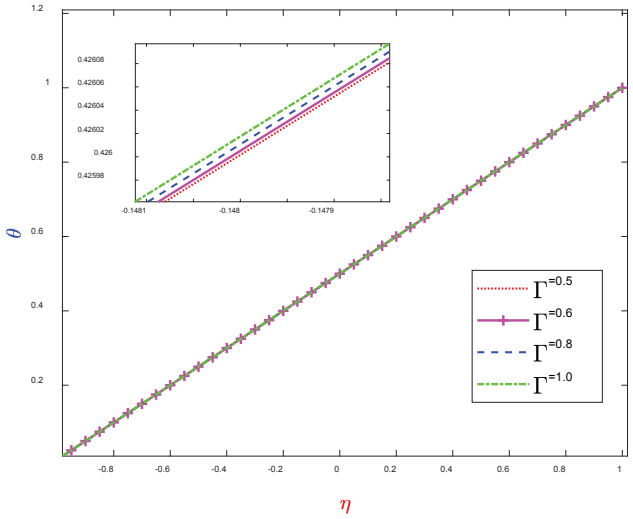

Figure 10. Effect of the nano layer on the temperature profile.

Nanolayer influence on thermal distribution is reported in Figure 10. This shows that increasing the surface layer of the nanoparticle increases fluid temperature. Fluid conductivity increases through improved heat transfer between nanoparticles and fluid, as observed from the graph. Enhanced Nanolayer improves temperature distribution, which is in line with the result reported by Gosunkanda et al. [27]. This conclusion that nanolayer thickness is crucial to thermal conductivity is also supported and experimentally validated by Yu and Choi [51]. The impact of large nano particle size on the nanofluid is observed in Figure 11, which shows that increasing the size of the nano particle from 10nm to 40 nm lowers the thermal profile. This is due to the large surface area of nanoparticles. As separation distance between particle decreases with larger volume concentration, which increases the heat transfer rate, consequently reducing the thermal boundary layer, thus temperature. This agrees with the conclusion by Yu and Choi [51] using experiment, that nanolayer thickness is crucial to thermal enhancement. Volumetric increase of nanoparticles from 1 to 8 % is reported in Figure 12, shows that nanoparticles have a significant influence on thermal distribution. As observed, temperature rise is due to enhanced thermal conductivity from nanoparticle to the base fluid. With higher particle concentration increase, the Van der Waals attractive potential may dominate electro-static repulsive potential, which may cause fluid particles to agglomerate [62]. Heat generation parameter influence on thermal distribution is shown in Figure 13. Heat generation internally is a cumulative effect of thermal energy sources including viscous dissipation and chemical reaction within the fluid. As observed from the graph, increased heat source improves fluid temperature, this is expected as heat generation reduces the thermal layer thickness, thus temperature is higher.

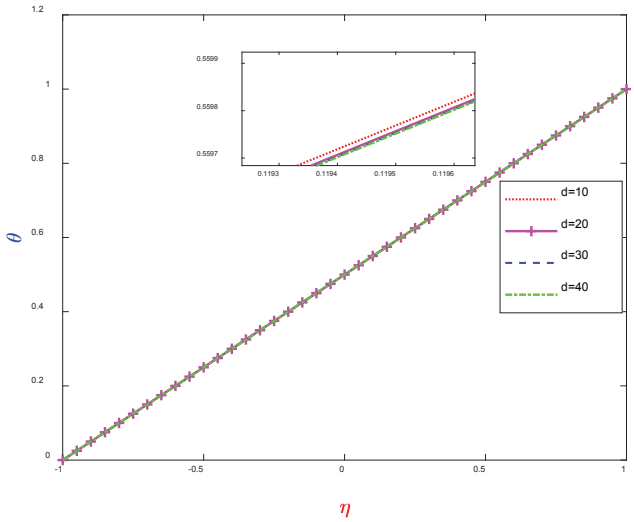

Figure 11. Effect of nanoparticle size on temperature profile.

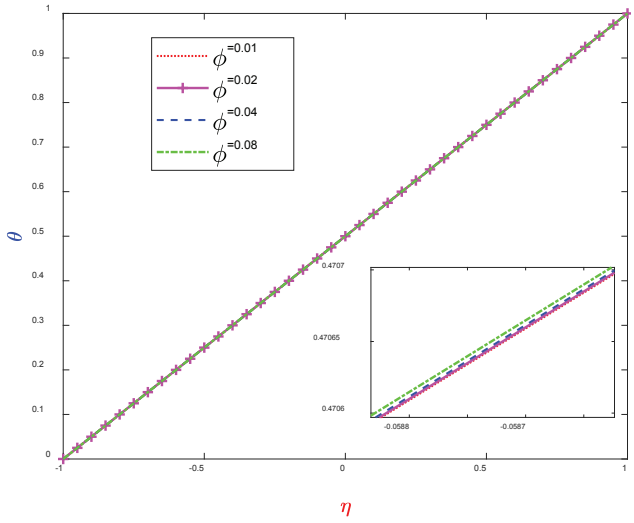

Figure 12. Effect of nanoparticle volume on temperature profile.

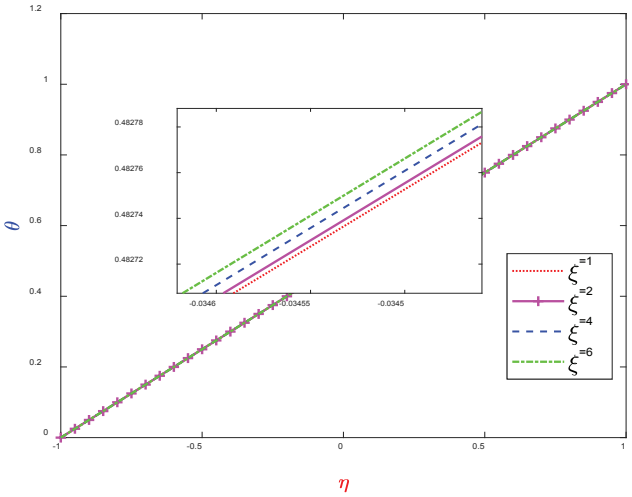

Figure 13. Effect of heat generation on temperature profile.

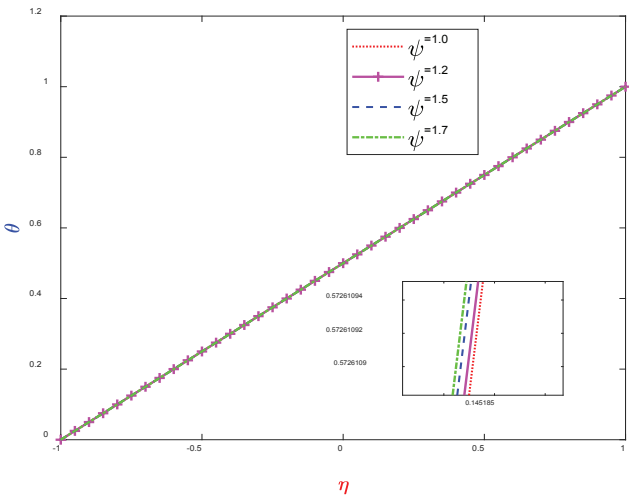

Figure 14. Effect of interparticle spacing on temperature profile.

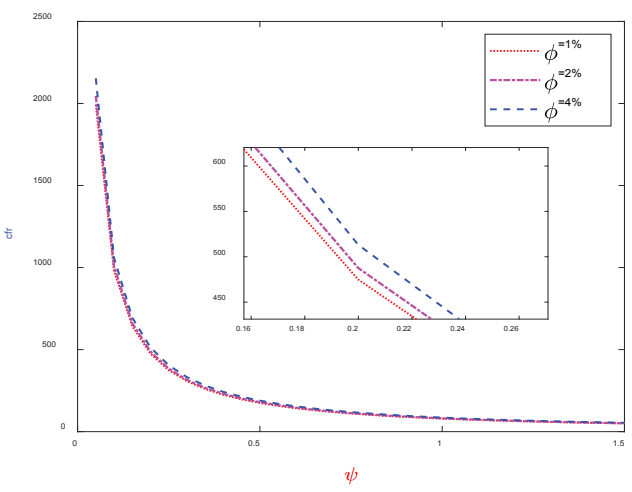

Figure 15a. Effect of copper nanoparticle volume and interparticle spacing on Skin friction.

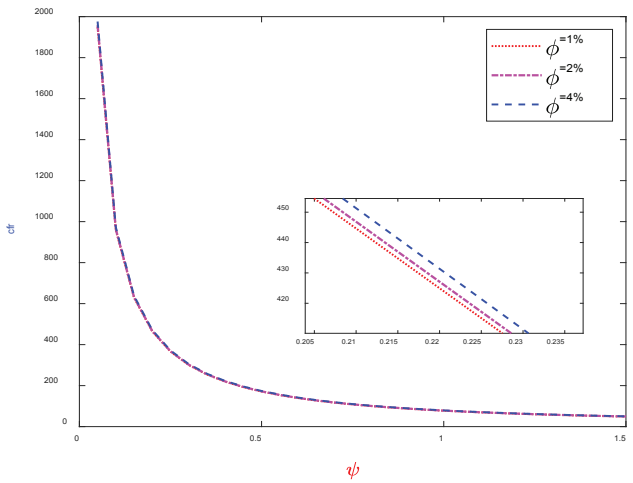

Figure 15b. Effect of graphite nanoparticle volume and interparticle spacing on Skin friction.

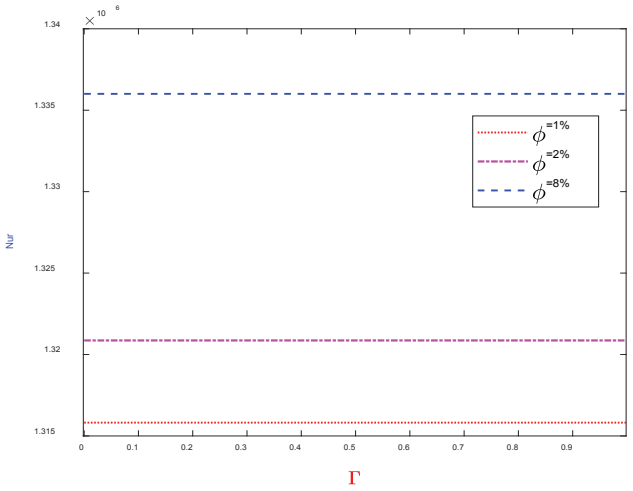

Figure16a. Effect of copper nanoparticle volume and size on Nusselt number.

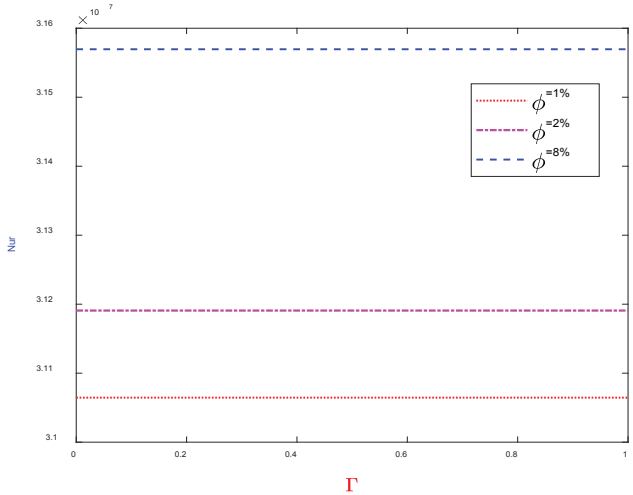

Figure 16b. Effect of graphite nanoparticle volume and size on Nusselt number.

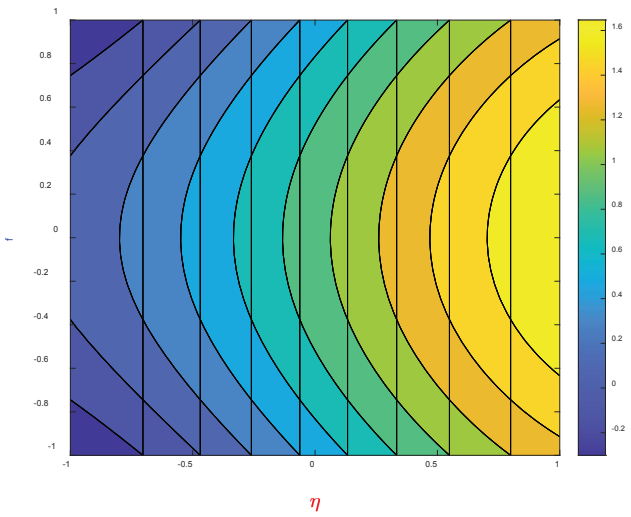

Figure 17. Contour plot of the velocity profile.

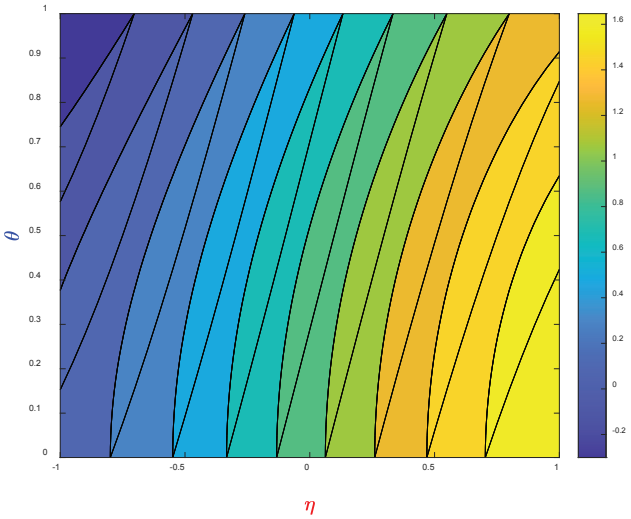

Figure 18. Contour plot of the temperature profile.

The effect of inter-particle spacing on thermal distribution is shown in Figure 14. This shows thermal distribution increases, as heat exchange between fluid molecules become more efficient. Further, the increase in particle separation distance implies lower Van der Waals attractive potential. If this potential is unable to dominate electrostatic repulsive potential the fluid is more stable [62]. Figure 15 shows the effect of nanoparticle volume and inter-particle spacing on skin friction, both on copper and graphite particles, as observed from the graphical representation larger volume of nanoparticles (1 – 8 %) increases skin friction which is highest at particle spacing of approximately 0.1 nm. This can be physically explained due to the larger particle volume increases shear stress between fluid layers, which causes dissipation of energy between the fluid and the boundary walls of the channel. Also, inter-particle spacing, which describes the gap between particles, shows that graphite has lower skin friction compared to copper particles as the gap widens between particles. The Nusselt number effect is shown in Figure 16 for both copper and graphite nanoparticles. As observed from the plot, nanoparticle volume concentration ranging from 1 – 8 % increases the heat transfer across the fluid channel, which can be explained due to the solid particle increase of fluid thermal conductivity. Consequently, heat transfer improves, with graphite having higher thermal characteristics compared to copper particles. However, a limitation which is not considered is particle agglomeration/ sedimentation. High thermal conductivity has been discussed as the focal point for high rate of heat transfer noticed. This might be impacted by nanoparticle agglomeration/sedimentation which increases heat potential energy, therefore heat conduction. This limitation can be addressed through the use of mechanical or chemical stability enhancement techniques to ensure uniform nanoparticle dispersion, which has been described thoroughly in [59]. The contour plot of the flow profile is shown in Figure 17; This is a graphical expression of the magnetic field intensity on the nano-mix flows through the microchannel. Shear stress equally plays a key role, as momentum is highest at the inner walls of the plate. The temperature profile contour plot is seen in Figure 18, as shown; the thermal distribution is higher at the upper plate. This is due to the influence of increased flow in this region.

PRACTICABILITY OF STUDY

The practicability of nanofluid flow in microchannel is an essential requirement, which should be discussed as it pertains to the system performance. Based on the aforementioned flow/operating conditions the impact of thermal variation, magnetic field and shearing as it may impact this study will be discussed.

The effect of thermal variation on the nanofluid is significant as it may cause nanoparticles to agglomerate, which is undesired. High temperature distribution leads to rapid movement of suspended particles, this is accounted for by the Brownian motion. Since high fluid temperature which increases the Brownian motion is also directly proportional to coefficient of diffusion, which causes particles to agglomerate. Addition of surfactant and polymers to nanoparticles have been reported [60-61] to mitigate agglomeration, however treating nanoparticle using plasma and mechanical techniques can help stabilize particles and prevent degradation at high temperature [62].

Several studies have reported nanoparticles agglomerate due to the application of magnetic field [63-64]; this may be due to decreasing particle repulsive potential which leads to particle aggregation. Study [65] suggest the use of oleic acid as dispersant, to help maintain particle stability under magnetic force field.

The effect of shear may be pronounced on nanofluid flow through micron sized channel, as it impact fluid viscosity.

High shearing leads to nanoparticle cluster breakdown. Long shear period may cause cluster to rebuild causing drag. Surfactant and polymer may be used as drag reducing agents or stabilizers. Due to its ability to alters the rheological and chemical nature of the fluid at boundary walls [62].

CONCLUSION

This paper examines the impact of nanoscale relations and heat generation on the thermal fluid transport of mineral oil in a microchannel. The mineral oil base fluid contains metallic and non-metallic particles of copper and graphite, respectively, considering the interfacial layer, which explains the anomalous increase in thermal conductivity of the nanofluid. The effect of fluid rheological parameters such as nano layer, particle size, interparticle spacing, thermal generated heat, and concentration volume of nanoparticles is evaluated on heat transfer and fluid transport. These are developed using nonlinear, higher-order differential models analyzed using the homotopy perturbation method, an analytical method. Results obtained from the study show:

i. A larger nano layer increases the surface layer contact between fluid and particles, consequently improving thermal distribution in the fluid.
ii. High volume of the nanoparticle concentration enhances heat transfer, as particles become more thermally conductive, with graphite having a higher heat transfer rate to copper.
iii. A higher particle concentration increases shear stress at the boundary, with copper having higher stress than graphite.
iv. High heat generation depletes the thermal boundary layer, raising the thermal transfer between the fluid and the channel surface.

This study may provide useful insight into mineral oil applications, including transformer cooling and lubrication in compressors amongst others. Further, since particle interaction, size and density are considered factors affecting nanofluid stability [59]. An interesting future outlook worthy of investigation will be the nanoscale relations effect on nanofluid stability.

AUTHORSHIP CONTRIBUTIONS

A.T. Akinshilo: Conceptualization, methodology/ Analysis, Investigation, Writing.
M.G. Sobamowo :Analysis
L. Kolsi: Validation

DATA AVAILABILITY STATEMENT

The authors confirm that the data that supports the findings of this study are available within the article. Raw data that support the finding of this study are available from the corresponding author, upon reasonable request.

CONFLICT OF INTEREST

The author declared no potential conflicts of interest with respect to the research, authorship, and/or publication of this article.

ETHICS

There are no ethical issues with the publication of this manuscript.

STATEMENT ON THE USE OF ARTIFICIAL INTELLIGENCE

Artificial intelligence was not used in the preparation of the article.

NOMENCLATURE

Re	Reynolds number
M	Magnetic Parameter
Γ	Interfacial layer (nm)
d	Diameter of the nanoparticle (nm)
Pr	Prandtl number
ϕ	Nanoparticle concentration
Nr	Radiation parameter
χ	Micropolar parameter
ξ	Heat generation parameter
β	Nanolayer ratio
γ	Ratio of interfacial layer thickness to particle size
ψ	Interparticle spacing (nm)
Nu	Nusselt number
(u,v)	Velocity components (m/s)
T	Nanofluid Temperature (K)
T_∞	Temperature away from the surface (K)
B_0	Magnetic field $(\Omega^{1/2})\ m^{-1}\ s^{1/2}\ kg^{1/2}$)
q_r	Radiative heat flux Kg/s^3
$\sigma^\star$	Stefan Boltzmann constant $Wm^{-2}\ k^{-4}$
k*	Mean absorption coefficient m^{-1}
ρ	Density kg/m^3
μ	Dynamic viscosity $kgm^{-1}\ s^{-1}$
ν	Kinematic viscosity $m^2\ s^{-1}$
k	Thermal conductivity $Wm^{-1}\ k^{-1}$
(ρC_p)	Heat capacitance $Jm^{-3}\ k^{-1}$
σ	Electrical conductivity Sm^{-1}
v_0	Suction/injection velocity m/s

REFERENCES

[1] Eli W. Nanofluid enhancement of mineral oil and thermal properties instrument design [Master's thesis]. University of Louisville; 2014.
[2] Nazir U, Sohail M, Naz S, Mukdasai K, Singh M, Singh A, et al. Effective role of mineral oil and biological nanometer on thermal energy influenced by magnetic dipole and nanoparticle. Front Mater 2023;10:22-33. [CrossRef]

[3] Jashi Y, Zanwar D, Gupta V. Influence of nanoparticle concentration on thermophysical properties and heat transfer performance of Al2O3 nanosuspension for refrigeration system. Mater Today Proc 2022;56(2):995-1000. [CrossRef]
[4] Khoirudin, Sukarman A, Abdulah B, Kristiawan AT, Wijayanta K, Enoki. The influence of nanofluids on thermal and electrical properties in mineral oil. In: The 5th Asean UEC Workshop 3; 2023; Bangkok, Thailand.
[5] Taheri AA, Abdali A, Taghilou M, Alhelou HH, Mazlumi K. Investigation of mineral oil based nanofluids effect on oil temperature reduction and loading capacity increment of distribution transformers. Energy Rep 2021;7:4325-4334. [CrossRef]
[6] Karaman HS, El-Dein AZ, Mansour DA, Lehtonen M, Darwish MMF. Influence of mineral oil based nanofluid oil based nanofluids on temperature distribution and generated heat energy inside minimum oil circuit breaker in making process. Nanomaterials 2023;13:1-19. [CrossRef]
[7] Shelton J, Saini NK, Hasan SM. Experimental study of rheological behavior of TiO2-Al2O3/mineral oil hybrid nanofluid. J Mol Liq 2023;380(15):121688. [CrossRef]
[8] Saman NM, Zakaria IH, Ahmad MH, Abdul-Malek Z. Effects of plasma treated alumina nanoparticles on breakdown strength, particle discharge resistance and thermophysical properties of mineral oil-based nanofluids. Materials 2021;14:1-27. [CrossRef]
[9] Khan H, Haneef M, Shah Z, Muhammad S, Islam S, Khan W. The combined magneto hydrodynamic and electric field effect on unsteady Maxwell nanofluid flow over a stretching surface under the influence of variable heat and thermal radiation. Appl Sci 2018;8(2):160. [CrossRef]
[10] Mahanthesh B, Gireesha BJ, Animasaun IL. Exploration of non-linear thermal radiation and suspended nanoparticles effects on mixed convection boundary layer flow on nano liquids on a melting vertical surface. J Nanofluids 2018;7(5):833-843. [CrossRef]
[11] Mahian O, Bellos E, Markides CN, Taylor RA, Alagumalai A, Yang L, et al. Recent advances in using nanofluids in renewable energy systems and the environmental implications of their uptake. Nano Energy 2021;86:106069. [CrossRef]
[12] Azwadi N, Sidik C, Samion S, Ghaderian J, Muhammad Yazid MNAW. Recent progress on the application of nanofluids in minimum quantity lubrication machining: A review. Int J Heat Mass Transf 2017;108(Part A):79-89. [CrossRef]
[13] Akinshilo AT. Thermal performance evaluation of MHD nanofluid transport through a rotating system undergoing uniform injection/suction with heat generation. BioNanoScience 2019;9(3):740-748. [CrossRef]
[14] Akinshilo AT. Mixed convective heat transfer analysis of MHD fluid flowing through an electrically conducting and non-conducting walls of a vertical micro-channel considering radiation effect. Appl Therm Eng 2019;156:506-513. [CrossRef]
[15] Venkat Kiran KU, Azenkeng A, Roy S. Exploring the potential of coal derived graphite as next generation lubricant additive for multifunctional applications. Manuf Lett 2024;14(Supplement):296-303. [CrossRef]
[16] Guo Z, Zhang Y, Wang J, Gao C, Zhang S, Zhang P, et al. Interactions of Cu nanoparticles with conventional lubricant additives on tribological performance and some physicochemical properties of an ester base oil. Tribol Int 2020;141:105941. [CrossRef]
[17] Dogonchi AS, Ganji DD. Study of nanofluid flow and heat transfer between non-parallel stretching walls considering Brownian motion. J Taiwan Inst Chem Eng 2016;69:1-13. [CrossRef]
[18] Dogonchi AS, Ganji DD. Investigation of MHD nanofluid flow and heat transfer in a stretching/shrinking convergent/divergent channel considering thermal radiation. J Mol Liq 2016;220:592-603. [CrossRef]
[19] Sathish Kumar M, Sandeep N, Rushi Kumar B, Viljayaragavan R. Effect of nonlinear thermal radiation on MHD Siko nanofluid flow over a bidirectional stretching surface. IOP Conf Ser Mater Sci Eng 2017;263:062023. [CrossRef]
[20] Mabood F, Akinshilo AT. Stability analysis and heat transfer of hybrid Cu-Al2O3 nanofluids transport over a stretching surface. Int Commun Heat Mass Transf 2021;123:105215. [CrossRef]
[21] Hdiri N, Souayeh B, Alfannakh H, Beya BB. Natural convection study with internal heat generation on heat transfer and fluid flow within a differentially heated square cavity filled with different working fluids and porous media. BioNanoScience 2019;9:702-722. [CrossRef]
[22] Maxwell JC. A Treatise on Electricity and Magnetism. Vol. 1. Oxford: Clarendon Press; 1873.
[23] Hamilton RL, Crosser OK. Thermal conductivity of heterogeneous two-component systems. Ind Eng Chem Fundam 1962;1(3):187-191. [CrossRef]
[24] Acharya N, Mabood F, Shahzad SA, Badruddin IA. Hydrothermal variations of radiative nanofluid flow by the influence of nanoparticles diameter and Nanolayer. Int Commun Heat Mass Transf 2022;130:105781. [CrossRef]
[25] Rana P, Beg OA. Mixed convection flow along an inclined permeable plate: Effect of magnetic field, Nanolayer, conductivity and nanoparticle diameter. Appl Nanosci 2015;5:569-581. [CrossRef]
[26] Graham AL. On the viscosity of suspensions of solid spheres. Appl Sci Res 1981:275-286. [CrossRef]
[27] Gosunkonda S, Gorti VPNS, Baluguri SB, Sakam SR. Particle spacing and chemical reaction effects on convective heat transfer through a nanofluid in cylindrical annulus. Procedia Eng 2015;127:263-270. [CrossRef]

[28] Eringen AC. Theory of micropolar fluids. J Math Mech 1966;16(1):1-18. [CrossRef]
[29] Afiridi MI, Qasim M. Entropy generation and heat transfer in boundary layer flow over a thin needle moving in a parallel stream in the presence of nonlinear Rosseland radiation. Int J Therm Sci 2018;123:117-128. [CrossRef]
[30] Sathish Kumar M, Sandeep N, Rushi Kumar B, Viljayaragavan R. Effect of nonlinear thermal radiation on MHD Siko nanofluid flow over a bidirectional stretching surface. IOP Conf Ser Mater Sci Eng 2017;263(06):60-65. [CrossRef]
[31] Nadeem S, Akram S. Peristaltic transport of a hyperbolic tangent fluid model in an asymmetric channel. Z Naturforsch A 2009;64:559-567. [CrossRef]
[32] Khedher NB, Mohammed HI, Abed AM, Biswas N, Togun H, Hammoodi KA, et al. Maximizing charging/discharging capabilities of horizontal shell-and-tube latent heat storage systems with innovative curved fin inserts. Int J Heat Mass Transf 2025;236(1):126289. [CrossRef]
[33] Sohrabi N, Hammoodi KA, Hammoud A, Jasim DJ, Karouei SHH, Kheyri J, et al. Using different geometries on the amount of heat transfer in a shell and tube heat exchanger using the finite volume method. Case Stud Therm Eng 2024;55:104037. [CrossRef]
[34] Rashid FL, Dhaidan NS, Mahdi AJ, Kadhim SA, Hammoodi KA, Al-Obaidi MA, et al. Heat transfer enhancement of phase change materials using tree shaped fins: A comprehensive review. Int Commun Heat Mass Transf 2025;162:108573. [CrossRef]
[35] Ali AJ, Eddin BE, Al-Musawi STM, Majdi HS, Chaichan MT. Fe3O4 Au nanoparticles influence on bio-nanofluid thermal conductivity. J Therm Eng 2025;11(1):159-169. [CrossRef]
[36] Matthews J, Tella H. Unsteady magnetohydrodynamic free convection flow of Al2O3-Cu/water nanofluid over a permeable linear stretching sheet through a porous medium with viscous dissipation and heat source/sink. J Therm Eng 2025;11(2):344-356. [CrossRef]
[37] Khrishna Varma KPV, Venkateswarlu K, Kalyai T, Hemalatha S, Kumar PV. Numerical analysis of spiral tube heat exchanger circulated with zinc oxide nanofluids. J Therm Eng 2025;11(2):377-389. [CrossRef]
[38] Eriksen AB, Kosinski P, Balakin BV, Kosinska A. Experimental study of a direct absorption solar collector with stationary nanofluids. Energy Convers Manag 2024;23:100683. [CrossRef]
[39] Akinshilo AT, Folaranmi A, Ilegbusi AO. Theoretical study of the MWCNT particle layer and size impact on sodium alginate heat transfer. Phys Scr 2024;99(9):095238. [CrossRef]
[40] Phillips 66 Lubricants. Synthetic PAO-Based, Rust and Oxidation-Inhibited Air Compressor Oil. Available at: https://www.phillips66lubricants.com/product/syncon-r-o-oil-iso-vg-32-68/. Accessed on June 3, 2025.
[41] Bhattacharjee B, Chakraborti P, Choudhuri K. Theoretical analysis of single-layered porous short journal bearing under the lubrication of micropolar fluid. J Braz Soc Mech Sci Eng 2019;41:365. [CrossRef]
[42] Ramzan M, Javed M, Rehman S, Saeed A, Kumam P, Galal AM. Irreversibility analysis of melting rheology in micropolar Al2O3 - mineral oil nanofluid with homogeneous and heterogeneous reaction. Numer Heat Transf A Appl 2024;85(3):444-466. [CrossRef]
[43] Akinshilo AT, Sobamowo MG, Adingwupu A. Evaluation of micropolar fluid transport through penetrable medium: Effect of flow and thermal slip. AUT J Mech Eng 2022;6(3):427-442.
[44] Alizadeh M, Dogonchi AS, Ganji DD. Micropolar nanofluid flow and heat transfer between penetrable walls by the presence of thermal radiation and magnetic field. Case Stud Therm Eng 2018;12:319-322. [CrossRef]
[45] Akinshilo AT, Ilegbusi AO, Ali HM, Sanusi M, Sobamowo MG. Impact of melting and radiation on MHD mixed convective heat transfer slip flow through vertical porous embedded micro channel. J Cent South Univ 2023;30:3670-3681. [CrossRef]
[46] Phillips 66 Lubricants. Heat Transfer Oil. Available at: https://www.phillips66lubricants.com/product/heat-transfer-oils/. Accessed on August 8, 2024.
[47] Kazaz O, Karimi N, Paul MC. Reduction and nanoparticle interaction for enhanced light absorption and heat conversion. J Mol Liq 2024;411:125702. [CrossRef]
[48] Wan J, Benson B, Bruzek MJ, Anthony JE, Sinko PJ, Prudhomme RK, et al. Microfluidic generation of droplet with high loading of nanoparticles. Langmuir 2012;18(37):13143-13148. [CrossRef]
[49] Li H, Li Y, Huang B, Xu T. Flow characteristics of the entrance region with roughness effect within rectangular microchannels. Micromachines 2020;11(1):30. [CrossRef]
[50] Yu CJ, Richter AG, Datta A. Molecular layering, a liquid on a solid substrate on X-ray reflectivity study. Physica B 2000;281(1-3):27-31. [CrossRef]
[51] Yu W, Choi SUS. The role of interfacial layer in the enhanced thermal conductivity of nanofluids: A renovated Maxwells model. J Nanopart Res 2003;5:167-171. [CrossRef]
[52] Karim KE, Kim B. First law of thermodynamics on the boundary flow through a carbon nanotube. Phys Rev E 2021;103:053115. [CrossRef]
[53] Babu JS, Sathian SP. The role of activation energy and reduced viscosity on the enhancement of water flow through carbon nanotubes. J Chem Phys 2011;134:194509. [CrossRef]
[54] Faramani AB, Aluru NR. Existence of multiple phases of water at nanotube interfaces. J Phys Chem 2016;120:23763-23771. [CrossRef]

[55] He JH. Homotopy perturbation method for solving boundary value problems. Phys Lett A 2006;350:87-88. [CrossRef]

[56] He JH. Homotopy perturbation method: A new nonlinear analytical technique. Appl Math Comput 2003;135:73-79. [CrossRef]

[57] Park J, Kim D, Kim H, Lee J, Chung W. Thermal radiative copper oxide layer for enhancing heat dissipation of metal surface. Nanomaterials 2021;11(11):2819. [CrossRef]

[58] Ouyang W, Qin H, Urbakh M, Hod O. Controllable thermal conductivity on twisted homogeneous interfaces of graphene and hexagonal boron nitride. Nano Lett 2020;20(10):7513-7518. [CrossRef]

[59] Khoirudin, Kristiawan B, Sukarman, Abdulah A, Santoso B, Wijayanta AT, et al. Flash point improvement of mineral oil utilizing nanoparticles to reduce fire risk in power transformers: A review. Fire 2024;7(305):1-25. [CrossRef]

[60] LotfizadehDehkordi B, Kazi S, Hamdi M, Ghadimi A, Sadeghinezhad E, Metselaar H. Investigation of viscosity and thermal conductivity of alumina nanofluids with addition of SDBS. Heat Mass Transf 2013;49:1109-1115. [CrossRef]

[61] Shanbedi M, Zeinali Heris S, Maskooki A. Experimental investigation of stability and thermophysical properties of carbon nanotubes suspension in the presence of different surfactants. J Therm Anal Calorim 2015;120:1193-1201. [CrossRef]

[62] Chakraborty S, Panigrati PK. Stability of nanofluid: A review. Appl Therm Eng 2020;174:115259. [CrossRef]

[63] Andreu JS, Camacho J, Faraudo J. Aggregation of superparamagnetic colloids in magnetic fields: The quest for the equilibrium state. Soft Matter 2011;7:2336-2339. [CrossRef]

[64] Ezzaier H, Marins JA, Claudet C, Hemery G, Sandre O, Kuzhir P. Kinetics of aggregation and magnetic separation of multicore iron oxide nanoparticles: Effect of the grafted layer thickness. Nanomaterials 2018;8:623. [CrossRef]

[65] Teng X, Yang H. Effects of surfactants and synthetic conditions on the sizes and self-assembly of monodisperse iron oxide nanoparticles. J Mater Chem 2004;14:774. [CrossRef]